Environmental Science
Water Research & Technology

Emerging investigators series: ultraviolet and Free Chlorine Aqueous-phase Advanced Oxidation Process: Kinetic Simulations and Experimental Validation

Journal:	*Environmental Science: Water Research & Technology*
Manuscript ID	EW-ART-03-2018-000196.R1
Article Type:	Paper
Date Submitted by the Author:	14-May-2018
Complete List of Authors:	Kamath, Divya; Michigan Technological University Minakata, Daisuke; Michigan Technological University,

An elementary reaction based kinetic model provides mechanistic insight into the reaction mechanisms induced by both hydroxyl and chlorine radicals and can be used as a comprehensive predictive model for any other compounds in the application of aqueous-phase ultraviolet combined with free chlorine advanced oxidation process for direct potable reuse of reclaimed wastewater.

Emerging investigators series: ultraviolet and Free Chlorine Aqueous-phase Advanced Oxidation Process: Kinetic Simulations and Experimental Validation

Prepared for Environmental Science: Water Research & Technology

Divya Kamath[1] and Daisuke Minakata*[1]

[1]Department of Civil and Environmental Engineering
Michigan Technological University
1400 Townsend Drive, Houghton, Michigan 49931, USA

*Corresponding author: Phone: +1-906-487-1830; fax: +1-906-487-2943; Email address: dminakat@mtu.edu

Abstract

An emerging advanced oxidation process uses ultraviolet light and free chlorine to produce active hydroxyl radicals and chlorine-derived radicals to degrade a variety of organic compounds in water. The use of free chlorine and reactivity of chlorine-derived radicals with many organic compounds have raised concerns about the potential formation of toxic degradation byproducts, e.g., chlorinated byproducts. An elementary reaction-based kinetic model is an attractive and promising approach to predict the degradation of a target organic compound and its degradation products and to provide mechanistic insight into the reaction mechanisms. We developed a UV/free chlorine elementary reaction-based kinetic model for a test compound, acetone, and its transformation products. The elementary reaction pathways were predicted by quantum mechanical calculations, and the reaction rate constants were predicted using previously developed linear free energy relationships. Ordinary differential equations were generated and numerically solved to obtain the time-dependent concentration profiles of acetone and its transformation products. Our experimental results were used to validate the model.

Introduction

Ultraviolet (UV) light combined with free chlorine (UV/free chlorine) is an emerging advanced oxidation process (AOP) that produces active hydroxyl radicals ($HO^{\bullet}$) and chlorine radicals ($Cl^{\bullet}$) to degrade a variety of organic compounds in water [1-3]. The UV/free chlorine AOP is an attractive alternative to conventional UV or chlorination disinfection techniques because of the potential to degrade organic compounds via active radicals and the use of residual free chlorine as a secondary disinfectant [4,5]. The UV/free chlorine AOP has recently been shown to degrade some target organic compounds more efficiently than the UV/hydrogen peroxide AOP due to: (1) the larger molar absorptivity of HOCl/OCl^- (ε_{HOCl}=59 $M^{-1}cm^{-1}$ and ε_{OCl^-}=66 $M^{-1}cm^{-1}$ at 253.7 nm) [6,7] and (2) the contribution of chlorine-derived radicals (i.e., $Cl^{\bullet}$: 2.34 V versus SHE; $Cl_2^{\bullet-}$: 2.13 V; $ClO^{\bullet}$: 2.39 V) [8] to organic compound degradation. For example, UV/free chlorine AOP has been considered as an alternative AOP after RO in wastewater reclamation processes for potable reuse of treated wastewater aiming to degrade low molecular weight neutral trace organic compounds that may be present in the RO permeate. UV/free chlorine does not require the quenching of hydrogen peroxide residue in the current practice of UV/hydrogen peroxide AOP because free chlorine can be used as secondary disinfectant.

The use of free chlorine and the reactivity of chlorine-derived radicals with many organic compounds in UV/free chlorine AOP results in the potential formation of toxic degradation byproducts, such as chlorinated byproducts [9,10]. Consequently, experimental investigations on the formation of chlorinated byproducts from some organic compounds have become an active research area. Because a number of organic compounds are used and commercially produced [11], a kinetic model that predicts the fate of these degradation products is needed to preliminarily screen organic compounds and AOP designs.

An elementary reaction pathway-based kinetic model is an attractive and promising model that predicts the degradation of a target organic compound and the degradation products and provides mechanistic insight into the reaction mechanisms [12]. Many experiment-based kinetic models have been developed for UV/hydrogen peroxide AOPs based on experimentally identified reaction pathways, and the rate constants were determined by fitting the experimentally determined concentration profiles [13,14]. However, this type of kinetic model often simplifies the reaction pathways and fails to predict the degradation products of other compounds. In contrast, an elementary reaction pathway-based kinetic model contains all possible elementary reactions and can comprehensively predict the degradation pathways of organic compounds [12]. This is particularly important for the UV/free chlorine AOP because chlorine-derived radicals

are very selective and produce different products depending on the elementary reaction pathways [15]. For example, $Cl^{\bullet}$ reacts by abstracting a hydrogen (H) atom from a C-H bond and reacts with an alcohol functional group via a single electron transfer to produce an alkoxyl radical [16], while $HO^{\bullet}$ favorably abstracts a H atom from a C-H bond to produce a carbon-centered radical. While the overall reactivities of $Cl^{\bullet}$ and $HO^{\bullet}$ are very similar (e.g., second-order reaction rate constant, k=10^{8}-10^{9} $M^{-1}s^{-1}$) [17-19], their reaction products are different because of the different elementary reaction mechanisms. Thus, the potential formation of typical transformation products such as aldehydes, ketones and carboxylic compounds should be mechanistically understood because of the concern about their toxicity (e.g., halogenated acids).

Quantum mechanical calculations using *ab initio* and density functional theory (DFT) are attractive techniques to identify elementary reaction pathways by calculating the thermodynamic properties using statistical thermodynamics [20]. Our previous studies used this technique with an implicit solvation model [universal solvation model (SMD)] to identify thermodynamically favorable, aqueous-phase elementary reactions for a series of chlorine-derived inorganic reactions produced in the UV/free chlorine AOP [15]. We also calculated the aqueous-phase free energies of activation for a series of $Cl^{\bullet}$ reactions with approximately 30 aliphatic organic compounds and found the linear free

energy relationships (LFERs) that relate the free energies of activation to the experimental k_{exp} values for H-atom abstraction and Cl-adduct formation [15].

In this study, we developed an elementary reaction pathway-based kinetic model for a test compound, acetone, in the UV/free chlorine AOP. The $HO^{\bullet}$-induced elementary reaction pathways for acetone and the reaction rate constants have been previously investigated [12]. Thus, we focused on the reactions of chlorine-derived radicals with acetone and the degradation products. The ordinary differential equations (ODEs) were developed based on the theoretically identified elementary reaction pathways and reaction rate constants predicted by the LFERs and numerically solved to obtain the time-dependent concentration profiles of acetone and the degradation products. We also performed batch experiments with the UV/free chlorine AOP to validate the model simulation results.

Materials and methods

Chemicals

All chemicals were ACS grade except for the chemicals that were used for the analytical measurements (HPLC grade). Acetone (>99%), sodium hypochlorite (available chlorine 10-15%), formic acid (>95%), sodium chlorate, and potassium chloride were purchased from Sigma Aldrich. Acetic acid (glacial) and sodium thiosulfate were purchased from

111 Fisher Scientific. All solutions used during the experiment were prepared with ultrapure
112 water (> 18 Ω) generated from a MilliQ system.

113 Experimental procedures

114 The experiments were carried out using an apparatus equipped with a low-pressure UV
115 lamp (Atlantic UV) emitting photons at 254 nm. The intensity of the measured light was
116 4.18×10^{-8} einstein/L•s using an actinometry procedure [21]. The path length was
117 determined to be 44.24 cm based on the photolysis of dilute H_2O_2 [22]. The UV lamp was
118 housed in a double-walled quartz immersion well, and cooling water was passed through
119 the system to control the temperature. The temperature of the reactors was monitored,
120 and the temperature of the solutions did not change by more than 1 °C for the duration of
121 the experiments. A detailed description of this photoreactor setup is available [23]. A
122 67.5 μM solution of acetone was prepared, and sodium hypochlorite (NaOCl) was added
123 to obtain 150 μM (10.7 mg/L) of free chlorine. After initiating the experiment, the
124 solutions were sampled at different time intervals. These samples were transferred to
125 vials containing a sodium thiosulfate solution (approximately 220 μM) to quench the
126 chlorine and terminate further reactions. All chemical analyses to measure the acetone
127 and transformation byproducts were performed within 24 h of the experiment.

Analytical methods

Acetone was measured using direct aqueous injection on a gas chromatograph (GC) equipped with a flame ionization detector (FID) and column (8-ft × 0.1-in. ID, stainless-steel column) packed with 1% SP-1000 on Carbopak-B 60/80 mesh. The injector and detector temperatures were 200 °C and 220 °C, respectively. Helium was used as the carrier gas, and hydrogen and air were used for the flame. The analysis method was 60 °C for 2 min followed by a 60 min increase of 2 °C /min and holding at 120 °C for 6 min. The retention time of acetone in this method was 4.6 min. The free chlorine in the aqueous solution was measured using a chlorine meter (Hach DPD colorimeter). Transformation byproducts were measured using an ion chromatograph (Dionex ICS 2100 series, IonPac AS17-C anion exchange column, 4 mm). The eluent was a potassium hydroxide (KOH) solution. The flow rate was 1.5 mL/min, and the flow conditions were set as follows: 0-15 min, 1 mM KOH (isocratic); 15-20 min, 1-10 mM KOH (ramp); 20-25 min, 10 mM KOH (isocratic); 25-30 min, 10-15 mM KOH (ramp). The retention times for acetate, formate, chloride and chlorate were 7, 9, 15 and 21 min, respectively.

Computational studies

All of the *ab initio* molecular orbital and DFT-based quantum mechanical calculations were performed with the Gaussian 09 revision D.02 program [24] using the Michigan Tech high-performance cluster "Superior". The electronic structures of the molecules and radicals in the ground and transition states were optimized at the level of B3LYP/6-

31G(*2df,p*) implemented in Gaussian-4 theory (G4) [25] in both the gaseous and aqueous phases. The aqueous-phase calculations were performed using a universal solvation model (SMD) [26]. We previously verified the combination of G4 with the SMD model by successful applying the combination to other aqueous-phase, radical-involved reactions [27]. Finally, these elementary reactions and rate constants were used to generate the kinetic rate equations in the form of ODEs and were solved using a numerical solver based on the Adam-Gear method from IMSL Roguewave's solver suite [28] by modifying an original UV/H_2O_2 model without assuming constant pH at non-steady-state condition [29].

Results and discussion

Experimental product study

Figure 1 shows the time-dependent concentration profiles of the acetone, free chlorine, and transformation byproducts measured in this experiment. While the free chlorine was completely consumed after 60 min of UV irradiation, only 53.6% of the acetone was degraded. The acetone degradation ceased upon complete photolysis of free chlorine, and no further degradation was observed. This indicates that acetone degradation occurred via acetone directly reacting with free chlorine and/or the photolysis caused by free chlorine. Thermal degradation of acetone by free chlorine is possible only for the enolate form, and the reported acetone enolization is insignificant (k=0.173 $M^{-1}s^{-1}$) [30] during the observed experimental time. In the dark, only 3% acetone degradation was observed after 2 h. Thus, the degradation of acetone results from the photolysis of free chlorine. The initial 150 μM sodium hypochlorite solution contained 15 μM chlorate, 300 μM chloride, and a few micromoles of acetic acid and formic acid to reach the given pH. As we eliminated

all possible contamination from the vials, ultrapure water, source water, and ion chromatography measurements, the presence of chlorate, chloride, and trace organic acids seemed to result from the stock sodium hypochlorite chemical. For example, hypochlorite auto decomposes into chlorate [31], which is the method used to form chloride for bleach (NaOCl) production. Previous literature reported trace quantities of perchlorate measured by an ion chromatograph tandem mass spectrometer (0.0003 to 0.0005 μM for the method detection limit) [32]. However, we did not detect perchlorate in our free chlorine source due to the higher detection limit using ion chromatography (~ 1 μM). Accordingly, the initial concentrations of these species were at some levels.

(Figure 1 goes here)

Elementary reaction pathways and reaction rate constants

The $HO^{\bullet}$ and $Cl^{\bullet}$ produced from the photolysis of free chlorine react with the target compound, acetone, to generate Cl-derived radicals, such as $Cl_2^{\bullet-}$, $ClO^{\bullet}$, and $ClO_2^{\bullet}$. The $HO^{\bullet}$-induced elementary reaction pathways of acetone degradation have been previously identified, and an elementary reaction-based kinetic model has been proposed [12]. Table 1 summarizes the elementary reaction pathways that involve Cl-derived radicals with the theoretically calculated aqueous-phase free energy of reaction, $\Delta G_{\mathrm{aq,calc}}^{\mathrm{react}}$, and free energy of activation, $\Delta G_{\mathrm{aq,calc}}^{\mathrm{act}}$, values and the reaction rate constants. While the $\Delta G_{\mathrm{aq,calc}}^{\mathrm{react}}$ values indicate the thermodynamical feasibility of elementary reaction pathway (e.g., if the value is negative, the reaction is exothermic and thermodynamically favorable to occur), the $\Delta G_{\mathrm{aq,calc}}^{\mathrm{act}}$ values represent the kinetics. It should be noted that the kinetics overruns the thermodynamics for fast radical reactions. The $HO^{\bullet}$ and Cl-derived radicals react with

193 acetone via H-atom abstraction from a C-H bond in a methyl functional group to produce
194 a carbon-centered radical [15,17,18]. The $\Delta G^{act}_{aq,calc}$ values for the reactions of $HO^{\bullet}$ and $Cl^{\bullet}$
195 with acetone were previously determined to be 7 kcal/mol and 3.2 kcal/mol, respectively.
196 Our new calculations using the same method obtained a $\Delta G^{act}_{aq,calc}$ value of 7.8 kcal/mol
197 for $Cl_2^{\bullet-}$, 1.5 kcal/mol for $ClO^{\bullet}$, and 14.1 kcal/mol for $ClO_2^{\bullet}$. The second-order reaction
198 rate constant of $Cl_2^{\bullet-}$ with acetone was experimentally determined and is 1.4×10^3 $M^{-1}s^{-1}$
199 [33], which indicates the insignificant contribution of this reaction to the overall
200 degradation of acetone. However, as indicated by the $\Delta G^{act}_{aq,calc}$ value and postulated by
201 several other experimental studies [34-35], the reaction of $ClO^{\bullet}$ with acetone is not
202 insignificant. More discussion on the reactivity of $ClO^{\bullet}$ will be provided in the following
203 section and kinetic simulation section.
204 While Cl-derived radicals react with acetone initially, Cl-derived radicals also
205 react with the other transformation byproducts formed during the degradation of acetone.
206 For example, $Cl^{\bullet}$ and $ClO^{\bullet}$ abstract H atoms from a C-H bond in HCOOH and $HCOO^-$
207 with $\Delta G^{act}_{aq,calc}$ values of 15.0 kcal/mol and 21 kcal/mol, respectively. Additionally, $Cl^{\bullet}$
208 reacts with the OH functional group of HCOOH with a $\Delta G^{act}_{aq,calc}$ value of 6.0 kcal/mol by
209 forming a Cl-adduct and then transferring a single electron to produce the alkoxyl radical
210 $HCOO^{\bullet}$. Using the previously developed LFERs: $\ln k = -0.50\,\Delta G^{act}_{aq,calc} + 20.53$ for H-atom
211 abstraction and $\ln k = -0.95\,\Delta G^{act}_{aq,calc} + 23.43$ for Cl-adduct formation by $Cl^{\bullet}$ [15], the k_{cal}
212 values were estimated to be 4.56×10^5 $M^{-1}s^{-1}$ for the H-atom abstraction and 5.01×10^7 $M^{-1}s^{-1}$ for the Cl-adduct formation. The k_{exp} value is $(1.3\pm0.1)\times10^8$ $M^{-1}s^{-1}$, and Cl-adduct

214 formation is the dominant reaction. We obtained a similar result for the reaction of $Cl^{\bullet}$
215 with CH_3COOH.

216 The reactivity of $ClO^{\bullet}$ with organic compounds is not well understood. A very
217 limited number of k_{exp} values have been reported for ionized aromatic compounds, and
218 these values range from 10^7-10^9 $M^{-1}s^{-1}$. The upper limit of the k_{exp} values for aliphatic
219 compounds (e.g., formate ion) is reported to be 1×10^6 $M^{-1}s^{-1}$. Our series of theoretical
220 calculations results in a $\Delta G^{act}_{aq,calc}$ value of approximately 15-25 kcal/mol (Table 1). We
221 obtained a $\Delta G^{act}_{aq,calc}$ value of 1.5 kcal/mol for the reaction of $ClO^{\bullet}$ with acetone, but the
222 reason for this abnormally low free energy of activation is not clear.
223 (Table 1 goes here)

224 ## Acetone degradation simulation

225 ### Overall results

226 Based on newly identified and previously known elementary reaction pathways and the
227 predicted reaction rate constants, we developed a kinetic model by modifying a UV/H_2O_2
228 kinetic model. To validate the kinetic model, we first simulated the time-dependent
229 concentrations of various initial free chlorine concentrations and a target organic
230 compound, benzoic acid, in the presence or absence of *tert*-butanol (*t*-BuOH), which acts
231 as a radical scavenger for $HO^{\bullet}$, without accounting for the transformation byproducts.
232 The simulated concentration profiles were compared to those experimentally obtained
233 and reported in the literature [37] (Figures SI 1-4 of Supporting Information). *t*-BuOH is
234 known to scavenge $HO^{\bullet}$, but it also reacts with $Cl^{\bullet}$ via Cl-adduct formation followed by a
235 single electron transfer [15]. The presence of *t*-BuOH inhibits benzoic acid decay, which

is induced only by $HO^{\bullet}$; thus, the difference in the benzoic acid decay observed between the addition and non-addition of *t*-BuOH is due to the reaction with $Cl^{\bullet}$ [37].

Once we validated our kinetic model with the experimentally obtained concentration profiles of a parent compound and free chlorine at various concentrations in the presence or absence of chloride ion, we added the elementary reaction pathways for acetone degradation induced by both $HO^{\bullet}$ and $Cl^{\bullet}$ and the predicted reaction rate constants (Table 1 and Table S1 of Supporting Information). Acetone has a small molar absorptivity, ε=16 $M^{-1}cm^{-1}$, at 254 nm, and the degradation of acetone by photolysis is negligible. We solved the ODEs to predict the concentration profiles of acetone, free chlorine and the transformation byproducts. Figure 1 shows the simulated concentration profiles of acetone, free chlorine, acetic acid, formic acid, chlorate, and chloride. The sample deviation (SD) calculated using equation (1) indicates how much the predicted data deviate from the experimental data [27,38].

$$\mathrm{SD}_j = \sqrt{\frac{1}{N_j - 1}\sum_{i=1}^{N_j}\left(\frac{C_{\mathrm{exp},i} - C_{\mathrm{cal},i}}{C_{\mathrm{exp},0}}\right)^2} \quad (1)$$

where N_j is the total number of data points for compound *j*, $C_{\mathrm{exp},i}$ and $C_{\mathrm{calc},i}$ are the experimentally determined and simulated concentration at time point *i*, respectively, and $C_{\mathrm{exp},0}$ is the initial experimental concentration at time zero. The SD was 0.54 for free chlorine, 0.14 for acetone, 1.1 for acetic acid, 0.58 for formic acid, 0.21 for chlorate, and 0.014 for chloride. One example of how to calculate the SD for free chlorine was given in SI. Although we did not detect the formations of other transformation products, the simulated concentration profiles of hydroxylacetone, oxyalic acid, glycolic acid, pyruvic aldehyde, formaldehyde, and glyoxylic acid are shown in Figure 2 as a comparison to

those that were obtained from UV/hydrogen peroxide AOP. The concentrations of these transformation products were smaller by several magnitude of orders than those detected in UV/hydrogen peroxide. Figure S5 shows the predicted concentration of methanol.

Contribution of Cl-derived radicals to acetone degradation

The preliminary simulation of the acetone concentration profile included the reactions of $HO^{\bullet}$, $Cl_2^{\bullet-}$ and $Cl^{\bullet}$ (Figure 3) with acetone (SD of 0.23). However, the simulated acetone degradation was slower than the experimental observation, which indicated that acetone may be degraded by other active Cl-derived radicals, such as $ClO^{\bullet}$ and $ClOH^{\bullet-}$. The simulated concentrations of these two radicals in the absence of a target organic compound were approximately 10^{-9} M for $ClO^{\bullet}$ (Figure S6) and 10^{-16} M for $ClOH^{\bullet-}$ (Figure S7). These results further confirm that $ClO^{\bullet}$ is the active radical contributing to the degradation of acetone, which was supported by our theoretical calculation. The absolute reaction rate constants of $ClO^{\bullet}$ with 2,5 dimethoxybenzoate ions and benzoate are 7×10^{8} $M^{-1}s^{-1}$, and $< 3\times10^{6}$ $M^{-1}s^{-1}$, respectively. Because no rate constants for $ClO^{\bullet}$ with aliphatic compounds have been reported, we determined the reaction rate constants of $ClO^{\bullet}$ with acetone via fitting the experimentally determined concentration profile of acetone by minimizing the SD. The determined rate constant was 3×10^{4} $M^{-1}s^{-1}$. By including this rate constant for the acetone decay, the SD for acetone was 0.14.

Fate of the transformation byproducts

The transformation byproducts measured in the experiments included acetic acid, formic acid, chlorate, and chloride. We recently elucidated the fate of $HO^{\bullet}$-induced acetone degradation byproducts, including those from peroxyl radical reactions. In this study, we added the $Cl^{\bullet}$-induced reaction pathways and the reactions of $Cl^{\bullet}$ with the transformation

byproducts. Other than the reaction of $ClO^{\bullet}$ with acetone, we did not include the reactions of $ClO^{\bullet}$ with the transformation byproducts because the reaction rate constants are not known. This may have caused the larger SD values in the concentration profiles of acetic acid and formic acid. Our kinetic simulation also predicted other transformation byproducts (e.g., formaldehyde, pyruvic aldehyde, hydroxyacetone and pyruvic acid) that were experimentally identified in the UV/H_2O_2 AOP (Figures 5-7). These products were simulated at very low concentrations (~0.1 μM), and our analytical instruments did not detect these species because of the limitations of our detection capabilities.

Chloride was generated from the production of free chlorine, and the initial sample contained approximately 300 μM chloride. During the UV/free chlorine AOP, the increase in the chloride concentration was not significant, and a 24.9% increase was observed due to the decay of free chlorine. Chlorate, ClO_3^-, was mainly generated by the reaction of $HO^{\bullet}$ with the chlorine dioxide radical ($ClO_2^{\bullet}$) that was generated via the reaction of $HO^{\bullet}$ with the chlorite ion, ClO_2^-. ClO_2^- was generated by the disproportionation reaction of $ClO^{\bullet}$. Typically, 2 to 17% of photolyzed free chlorine is converted to ClO_3^-. In this study, 12% of the photolyzed free chlorine was converted to ClO_3^-, and ClO_3^- was present at a concentration of 2.5 mg/L until the free chlorine was completely consumed. No ClO_3^- degradation mechanisms are known. ClO_3^- is included in the contaminant candidate list (CCL 4) by the U.S. EPA [39], and a national guideline of 1 mg/L of ClO_3^- is used in Canada [40]. Thus, caution must be exercised when using free chlorine.

Conclusions

This study highlights the importance of an elementary reaction-based kinetic model for the UV/free chlorine AOP. The elementary reaction pathways and reaction rate constants were predicted by quantum mechanical calculations. ODEs were numerically solved to predict the concentration profiles of a target organic compound, acetone, and the transformation products. $ClO^{\bullet}$ was identified as a potential oxidant in this system because of its high concentration, and its reaction rate constant with acetone was determined to be 3×10^{4} $M^{-1}s^{-1}$. Chlorate formation was in the range of 2.5 mg/L with 10.7 mg/L of free chlorine. Although chlorate is not yet regulated, this may be a potential cause for concern when using this treatment technology.

Acknowledgements

This work was supported by the National Science Foundation Award: CBET-1435926. Any opinions, findings, conclusions, or recommendations expressed in this publication are those of the authors and do not necessarily reflect the views of the supporting organization. The authors appreciate the support from the Michigan Tech HPC cluster 'Superior'.

Figure Captions

Figure 1: Experimental and predicted time-dependent concentration profiles of acetone, acetic acid, formic acid, free chlorine, chlorate and chloride.

Figure 2: Predicted time-dependent concentration profiles of hydroxyacetone, oxalic acid, glycolic acid (left) and pyruvic aldehyde, formaldehyde, and glyoxylic acid (right)

Figure 3: Predicted time-dependent concentration profiles of $HO^{\bullet}$, $Cl^{\bullet}$ and $Cl_2^{\bullet-}$ radicals.

Table Caption

Table 1: Theoretically identified elementary reaction pathways and predicted reaction rate constants for Cl-derived radical reactions with organic compounds.

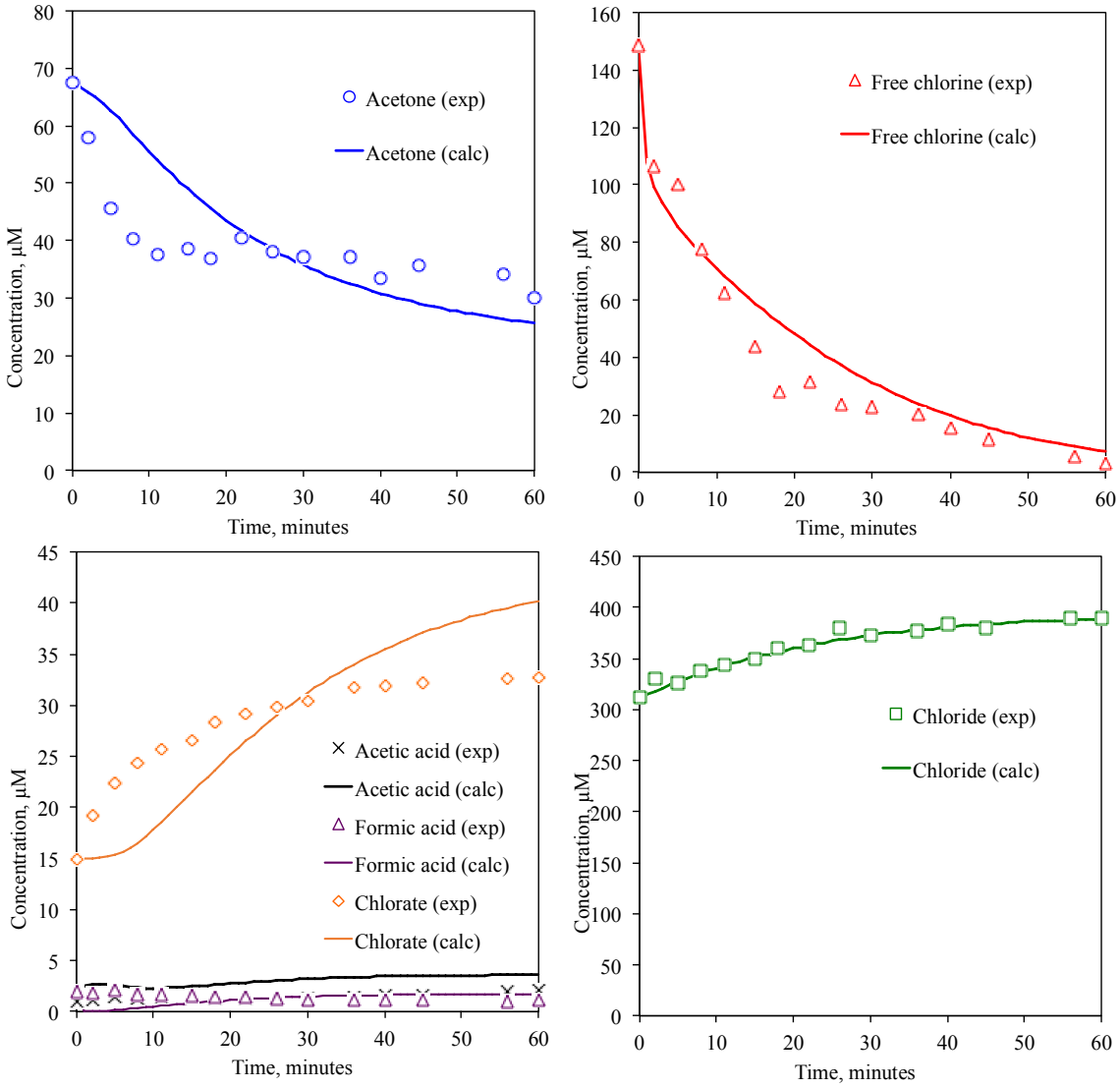

330

331 Figure 1

332

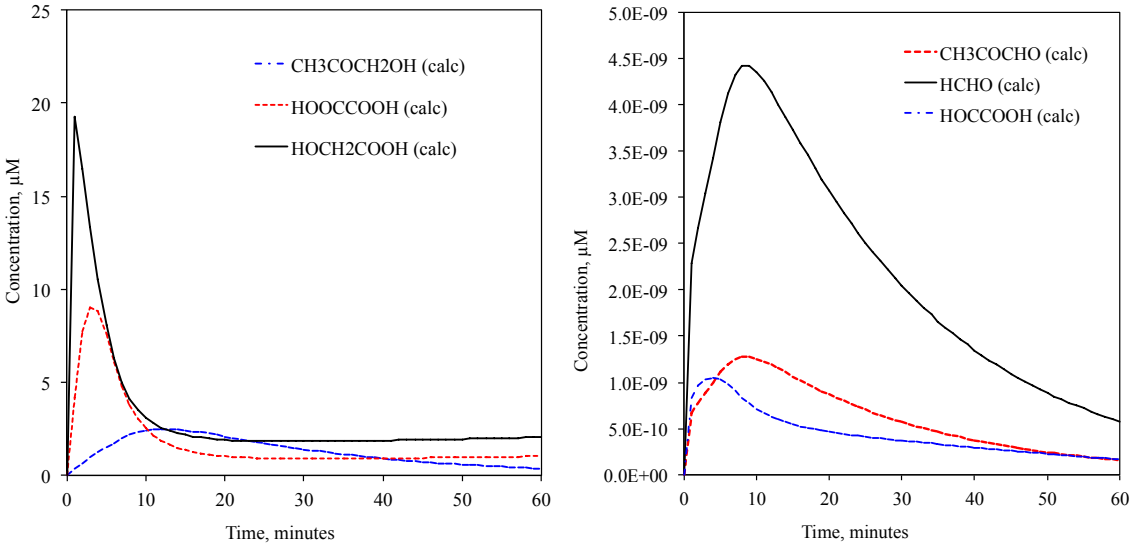

333

334 Figure 2

335

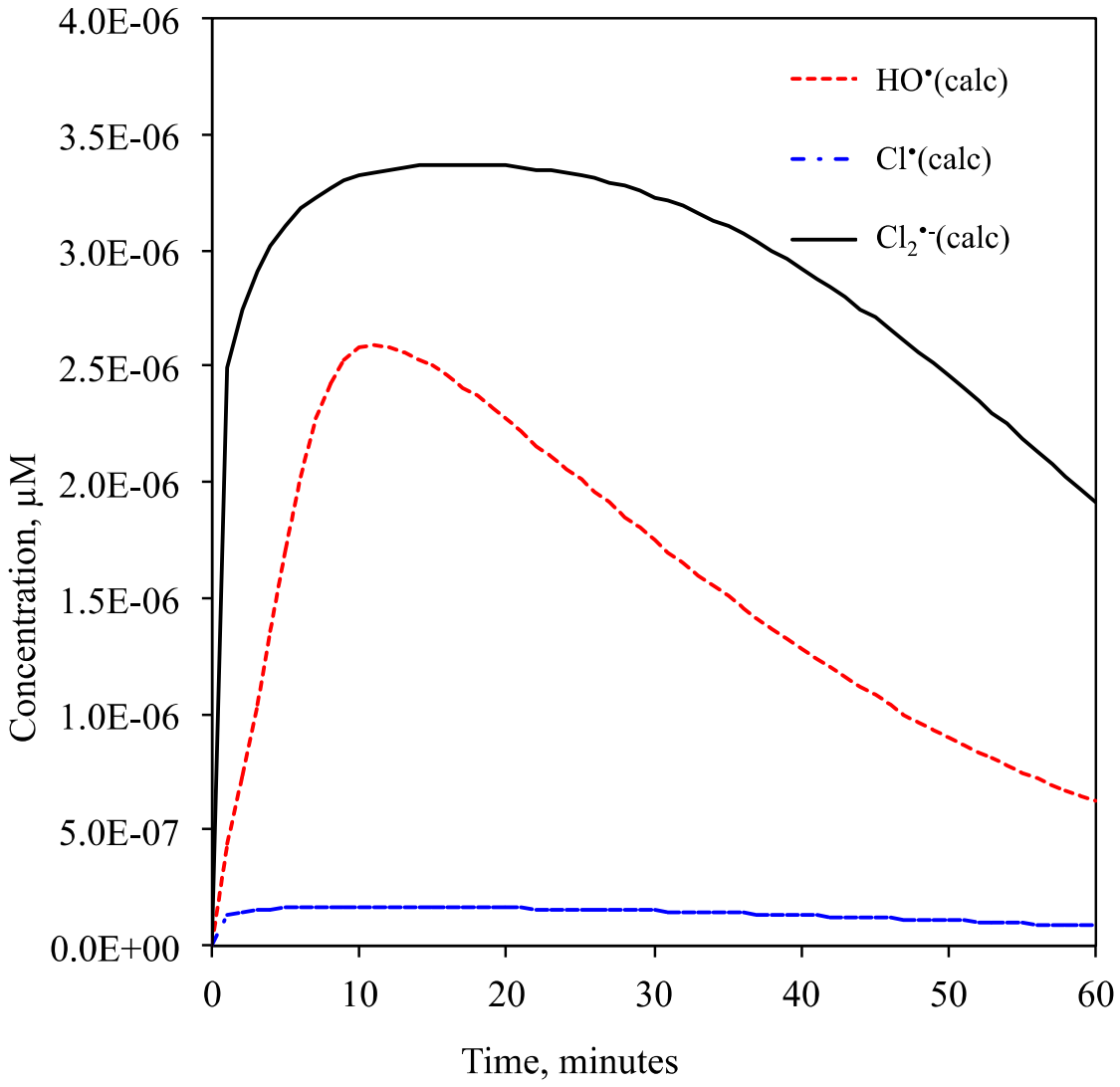
4.0E-06
3.5E-06
3.0E-06
2.5E-06
2.0E-06
1.5E-06
1.0E-06
5.0E-07
0.0E+00
Concentration, µM
0
10
20
30
40
50
60
Time, minutes
HO•(calc)
Cl•(calc)
Cl2•-(calc)

Figure 3

343 Table 1

Elementary reaction pathways	k_{exp} $M^{-1}s^{-1}$	k_{calc} $M^{-1}s^{-1}$	$\Delta G^{act}_{aq,calc}$ kcal/mol	$\Delta G^{react}_{aq,calc}$ kcal/mol
$CH_3COCH_3 + HO^{\bullet} \rightarrow {}^{\bullet}CH_2COCH_3 + H_2O$	1.1×10^8 [17]	7.5×10^7	7.0	-25.4 [12]
$CH_3COCH_3 + Cl^{\bullet} \rightarrow {}^{\bullet}CH_2COCH_3 + HCl$	$(7.8 \pm 0.7) \times 10^7$ [36]	1.66×10^8	3.2	-12.2 [15]
$CH_3COCH_3 + Cl_2^{\bullet-} \rightarrow {}^{\bullet}CH_2COCH_3 + HCl + Cl^-$	1.4×10^3 [33]		7.8*	
$CH_3COCH_3 + ClO^{\bullet} \rightarrow {}^{\bullet}CH_2COCH_3 + H^+ + OCl^-$		3.0×10^4	1.5	
$CH_3COCH_3 + ClO_2 \rightarrow {}^{\bullet}CH_2COCH_3 + HCl$		< 10	14.1	
$CH_3COCHO + Cl^{\bullet} \rightarrow {}^{\bullet}CH_2COCHO + HCl$		6.12×10^7	5.2	-1.5
$CH_3COCHO + ClO^{\bullet} \rightarrow {}^{\bullet}CH_2COCHO + H^+ + OCl^-$			20.0	-1.9
$CH_3COCH_2OH + Cl^{\bullet} \rightarrow {}^{\bullet}CH_2COCH_2OH + HCl$		1.75×10^8	3.1	-11.3
$CH_3COCH_2OH + ClO^{\bullet} \rightarrow {}^{\bullet}CH_2COCH_2OH + H^+ + OCl^-$			20.0	-11.7
$CH_3COCH_2OH + Cl^{\bullet} \rightarrow CH_3CO{}^{\bullet}CHOH + HCl$		6.77×10^7	5.0	-24.8
$CH_3COCH_2OH + ClO^{\bullet} \rightarrow CH_3CO{}^{\bullet}CHOH + H^+ + OCl^-$			14.4	-25.2
$CH_3COCH_2OH + Cl^{\bullet} \rightarrow CH_3COCH_2O({}^{\bullet}Cl)H$		7.88×10^8	3.1	0.74
$CH_3COCH(OH)_2 + Cl^{\bullet} \rightarrow {}^{\bullet}CH_2COCH(OH)_2 + HCl$		1.23×10^8	3.8	-12.8
$CH_3COCH(OH)_2 + ClO^{\bullet} \rightarrow {}^{\bullet}CH_2COCH(OH)_2 + H^+ + OCl^-$			18.5	-13.2
$CH_3COCH(OH)_2 + Cl^{\bullet} \rightarrow CH_3CO{}^{\bullet}CH(OH)_2 + HCl$			-18.8	-26.4
$CH_3COCH(OH)_2 + ClO^{\bullet} \rightarrow CH_3CO{}^{\bullet}CH(OH)_2 + H^+ + OCl^-$			14.7	-26.8
$CH_3COCH(OH)_2 + Cl^{\bullet} \rightarrow CH_3COCH(OH)O({}^{\bullet}Cl)H$		5.79×10^9	1.0	0.71
$CH_3COCOOH + Cl^{\bullet} \rightarrow {}^{\bullet}CH_2COCOOH + HCl$		3.53×10^7	6.3	-11.4
$CH_3COCOOH + ClO^{\bullet} \rightarrow {}^{\bullet}CH_2COCOOH + H^+ + OCl^-$			22.5*	-11.8

$CH_3COCOOH + Cl^{\bullet} \rightarrow CH_3COCO(^{\bullet}Cl)OH$		6.06×10^7	5.8	2.2
$CH_3COCOO^- + Cl^{\bullet} \rightarrow {}^{\bullet}CH_2COCOO^- + HCl$		9.34×10^8	-0.25	-1.57
$CH_3COCOO^- + ClO^{\bullet} \rightarrow {}^{\bullet}CH_2COCOO^- + H^+ + OCl^-$			2.5*	-1.95
$HCOOH + Cl^{\bullet} \rightarrow {}^{\bullet}COOH + HCl$	$(1.3 \pm 0.1) \times 10^8$ [18]	4.56×10^5	15.0	-3.5
$HCOOH + Cl^{\bullet} \rightarrow HCOO(^{\bullet}Cl)H$		5.01×10^7	6.0	37.2
$HCOOH + ClO^{\bullet} \rightarrow {}^{\bullet}COOH + H^+ + OCl^-$			21.0	-3.9
$HCOO^- + Cl^{\bullet} \rightarrow {}^{\bullet}COO^- + HCl$	$(4.2 \pm 0.5) \times 10^9$ [18]		-10.1	40
$HCOO^- + Cl^{\bullet} \rightarrow HCOO(^{\bullet}Cl)^-$		3.96×10^9	1.4	3.0
$HCOO^- + ClO^{\bullet} \rightarrow {}^{\bullet}COO^- + H^+ + OCl^-$			-6.4	39.1
$CH_3COOH + Cl^{\bullet} \rightarrow {}^{\bullet}CH_2COOH + HCl$	$(3.2 \pm 0.2) \times 10^7$ [18], $(1.0 \pm 0.2) \times 10^8$ [36]	5.82×10^7	5.3	-8.3
$CH_3COOH + Cl^{\bullet} \rightarrow CH_3COO(^{\bullet}Cl)H$		8.67×10^8	3.0	29.7
$CH_3COOH + ClO^{\bullet} \rightarrow {}^{\bullet}CH_2COOH + H^+ + OCl^-$			26.3*	-9.1
$CH_3COO^- + Cl^{\bullet} \rightarrow {}^{\bullet}CH_2COO^- + HCl$	$(3.7 \pm 0.4) \times 10^9$ [18]	5.15×10^8	0.94	-7.5
$CH_3COO^- + Cl^{\bullet} \rightarrow CH_3COO(^{\bullet}Cl)^-$		4.79×10^9	1.2	-3.3
$CH_3COO^- + ClO^{\bullet} \rightarrow {}^{\bullet}CH_2COO^- + H^+ + OCl^-$			18.7	-7.9
$CH_3OH + Cl^{\bullet} \rightarrow {}^{\bullet}CH_2OH + HCl$	$(1.0 \pm 0.2) \times 10^9$ [18], $(1.0 \pm 0.1) \times 10^9$ [36]	5.82×10^7	5.3	-5.0 [15]
$CH_3OH + Cl^{\bullet} \rightarrow CH_3O(^{\bullet}Cl)H$		9.53×10^8	2.9	27.1 [15]
$CH_3OH + ClO^{\bullet} \rightarrow {}^{\bullet}CH_2OH + H^+ + OCl$-			15.7	-5.4
$CH_3CHO + Cl^{\bullet} \rightarrow {}^{\bullet}CH_2CHO + HCl$	$(6.3 \pm 0.4) \times 10^8$ [18]	7.86×10^7	4.7	-0.89
$CH_3CHO + ClO^{\bullet} \rightarrow {}^{\bullet}CH_2CHO + H^+ + OCl^-$			-1.56	-1.27

344 *estimated based on the gaseous phase free energy of activation

References

1. C.K. Remucal, and D. Manley, Emerging investigators series: the efficacy of chlorine photolysis as an advanced oxidation process for drinking water treatment. *Environ. Sci.: Water Res. Technol*., 2016, **2**, 565-579.
2. M.J. Watts, E.J. Rosenfeldt, and K.G. Linden, Comparative OH radical oxidation using UV-Cl_2 and UV-H_2O_2 processes. *J. Water Supply Res. Technol. AQUA*., **2007**, 56 (8), 469-477.
3. M.J. Watts, and K.G. Linden, Chlorine photolysis and subsequent OH radical production during UV treatment of chlorinated water. *Wat. Res*., 2007, **41**, 2871-2878.
4. S. Rattanakul, and K. Oguma, Analysis of hydroxyl radicals and inactivation mechanisms of bacteriophage MS2 in response to a simultaneous application of UV and chlorine. *Environ. Sci. Technol*., 2017, **51**(1), 455-462.
5. W.L. Wang, Q.Y. Wu, N. Huang, T. Wang, and H.Y. Hu, Synergistic effect between UV and chlorine (UV/chlorine) on the degradation of carbamazepine: Influence factors and radical species. *Water Res.,* 2016, **98**, 190–198.
6. L.H. Nowell, and J. Hoigné, Photolysis of Aqueous Chlorine at Sunlight and Ultraviolet Wavelengths.1. Degradation Rates. *Water Res.,* 1992, **26**(5), 593–598.
7. L.H. Nowell, and J. Hoigné, Photolysis of Aqueous Chlorine at Sunlight and Ultraviolet Wavelengths. 2. Hydroxyl Radical Production. *Water Res.,* 1992, **26** (5), 599–605.
8. D.M. Stanbury, S. Steenken, and P. Wardman, Standard electrode potentials involving radicals in aqueous solution inorganic radicals. *Biolnorg React Mech*., 2013, **9**(1-4), 59-61.
9. D. Wang, J.R. Bolton, S.A. Andrews, and R. Hofmann, Formation of disinfection by-products in the ultraviolet/chlorine advanced oxidation process. *Sci. of the Total Environ*., 2015, **518-519**, 49-57.
10. Z. B. Guo, Y.L. Lin, B. Xu, H. Huang, T.Y. Zhang, F.X. Tian, and N.Y. Gao, Degradation of chlortoluron during UV irradiation and UV/chlorine processes and formation of disinfection by-products in sequential chlorination. *Chem. Eng. J.,* 2016, **283**, 412–419.
11. *CAS* Website; https://www.cas.org/ accessed in March 24, 2018.
12. D. Kamath, S. Mezyk, and D. Minakata, Elucidating the elementary reaction pathways and kinetics of hydroxyl radical-induced organic compound degradation in aqueous phase advanced oxidation processes. *Environ. Sci. Technol*., 2018, under revision.
13. M.I. Stefan, A.R. Hoy, and J.R. Bolton, Kinetics and mechanisms of the degradation and mineralization of acetone in dilute aqueous solution sensitized by the UV photolysis of hydrogen peroxide. *Environ. Sic. Technol*., 1996, **30**, 2382-2390.
14. M. Rodigast, A. Mutzel, J. Schindelka, and H. Herrmann, A new source of methylglyoxal in the aqueous phase. *Atmos. Chem. Phys*., 2016, **16**, 2689-2702.
15. D. Minakata, D. Kamath, and S. Maetzold, Mechanistic insight into the reactivity of chlorine-derived radicals in the aqueous-phase UV-chlorine advanced

oxidation process: quantum mechanical calculations. *Environ. Sci. Technol*., 2017, **51**, 6918-6926.

16. B.C. Gilbert, J.K. Stell, W.J. Peet, and K.J. Radford, Generation and reactions of the chlorine atom in aqueous solution. *J. Chem. Soc., Faraday Trans*. 1. 1988, **84** (10), 3319-3330.
17. G.V. Buxton, C.L. Greenstock, W.P. Helman, and A.B. Ross, Critical review of rate constants for reactions of hydrated electrons, hydrogen atoms and hydroxyl radicals (•OH/•O−) in aqueous solution. *J. Phys. Chem. Ref. Data.,* 1988, **17**, 513−886.
18. G.V. Buxton, M. Bydder, G.A. Salmon, and J.E. Williams, The reactivity of chlorine atoms in aqueous solution. *PCCP*., 2000, **2**, 237-245.
19. H. Herrmann, Kinetics of aqueous phase reactions relevant for atmospheric chemistry. *Chem. Rev*., 2003, **103**, 4691-4716.
20. J.W. Gibbs, Elementary Principles in Statistical Mechanics, 1902 Charles Scribner's Sons. New York.
21. S. Murov, I. Carmichael, and G.L. Hug, *Handbook of photochemistry*, 2nd ed.; Marcel Dekker Inc.: New York, NY, 1993.
22. T. Garoma, and M.D. Gurol, Process Using Oxalic Acid as Probe Chemical. *Environ. Sci. Technol.,* 2005, **39**(20), 7964–7969.
23. L. Varanasi, E. Coscarelli, M. Khaksari, L.R. Mazzoleni, and D. Minakata, Transformations of dissolved organic matter induced by UV photolysis, hydroxyl radicals, chlorine radcials, and sulfate radicals in aqueous-phase UV-based advanced oxidation processes. *Wat. Res*., 2018, **135**, 22-30.
24. M.J. Frisch, G.W. Trucks, H.B. Schlegel, G.E. Scuseria, M.A. Robb, J.R, Cheeseman, G. Scalmani, V. Barone, B. Mennucci, G.A. Petersson, H. Nakatsuji, Caricato, X. Li, H.P. Hratchian, A.F. Izmaylov, J. Bloino, G. Zheng, J.L. Sonnenberg, M. Hada, M. Ehara, K. Toyota, R. Fukuda, J. Hasegawa, M. Ishida, T. Nakajima, Y. Honda, O. Kitao, H. Nakai, T. Vreven, J.A. Montgomery, Jr., J.E. Peralta, F. Ogliaro, M. Bearpark, J.J. Heyd, E. Brothers, K.N. Kudin, V.N. Staroverov, R. Kobayashi, J. Normand, K. Raghavachari, A. Rendell, J.C. Burant, S.S. Iyengar, J. Tomasi, M. Cossi, N. Rega, N. J. Millam, M. Klene, J.E. Knox, J.B. Cross, V. Bakken, C. Adamo, J. Jaramillo, R. Gomperts, R.E. Stratmann, R. O. Yazyev, A.J. Austin, R. Cammi, C. Pomelli, J.W. Ochterski, R. Martin, K. Morokuma, V.G. Zakrzewski, G.A. Voth, P. Salvador, J.J. Dannenberg, S. Dapprich, A.D. Daniels, Ö. Farkas, J.B. Foresman, J.V. Ortiz, J. Cioslowski, and D.J. Fox, Gaussian 09, Revision D.1; Gaussian, Inc., Wallingford CT, 2009.
25. L.A. Curtiss, P.C. Redfern, and K. Raghavachari, Gaussian-4 theory. *J. Chem. Phys*., 2007, **126**, 084108.
26. A.V. Marenich, C.J. Cramer, and D.G. Truhlar, Universal solvation model based on solute electron density and on a continuum model of the solvent defined by the bulk dielectric constant and atomic surface tensions. *J. Phys. Chem*. B., 2009, **113**, 6378−6396.
27. D. Minakata, S.P. Mezyk, J.W. Jones, B.R. Daws, and J.C. Crittenden, Development of linear free energy relationships for aqueous phase radical-involved chemical reactions. *Environ. Sci. Technol*., 2014, **48**, 13925-13932.
28. Rogue Wave Software. Parallel Programming and the IMSL Libraries. 2012.

29. J.C. Crittenden, H. Hu, D.W. Hand, and S.A. Green, A kinetic model for H_2O_2/UV process in a completely mixed batch reactor. *Wat. Res*. 1999, **33**(10), 2315-2328.
30. J.P. Guthrie, and J. Cossar, The chlorination of acetone: a complete kinetic analysis. *Can. J. Chem.,* 1986, **64**, 1250–1266.
31. B.D. Stanford, A.N. Pisarenko, S.A. Snyder, and G.Gordon, Perchlorate, bromate , and chlorate in hypochlorite solutions : Guidelines for utilities. *J AWWA*, **103** (6), 71–83.
32. D. Wang, J.R. Bolton, S.A. Andrews, and R. Hofmann, Formation of disinfection by-products in the ultraviolet / chlorine advanced oxidation process. *Sci. Total Environ.,* 2015, **518–519**, 49–57.
33. K. Hasegawa, and P. Neta, Rate Constants and Mechanisms of Reaction of Cl2- Radicals. *J. Phys. Chem.,* 1978, **82**(8), 854–857.
34. K. Guo, Z. Wu, C. Shang, B. Yao, S. Hou, X. Yang, W. Song, and J. Fang, Radical chemistry and structural relationships of PPCP degradation by UV/chlorine treatment in simulated drinking water. *Environ. Sci. Technol*., 2017, **51**, 10431-10439.
35. X. Kong, Z. Wu, Z. Ren, K. Guo, S. Hou, Z. Hua, X. Li, and J. Fang, Degradation of lipid regulators by the UV/chlorine process: Radical mechanisms, chlorine oxide radical ($ClO^{\bullet}$)-mediated transformation pathways and toxicity changes. *Wat. Res*., 2018, **137**(15), 242-250.
36. F. Wicktor, A. Donati, H. Herrmann, and R. Zellner, Laser based spectroscopic and kinetic investigations of reactions of the Cl atom with oxygenated hydrocarbons in aqueous solution. *PCCP*., 2003, **3**, 2562–2572.
37. J. Fang, Y. Fu, and C. Shang, The roles of reactive species in micropollutant degradation in the UV/free chlorine system. *Environ. Sci. Technol.,* 2014, **48**(3), 1859–1868.
38. X. Guo, D. Minakata, J. Niu, and J. Crittenden, Computer-based first-principles kinetic modeling of degradation pathways and byproduct fates in aqueous-phase advanced oxidation procsses. *Environ. Sci. Technol.,* 2014, **48**, 5718-5725.
39. U.S. EPA. Chemical Contaminants –CCL4. Accessed on March 13, 2018: https://www.epa.gov/ccl/chemical-contaminants-ccl-4
40. *Guidelines for Canadian Drinking Water Quality : Guideline Technical Document Chlorite and Chlorate*; Ottawa, Ontario, 2008.

Table of Content

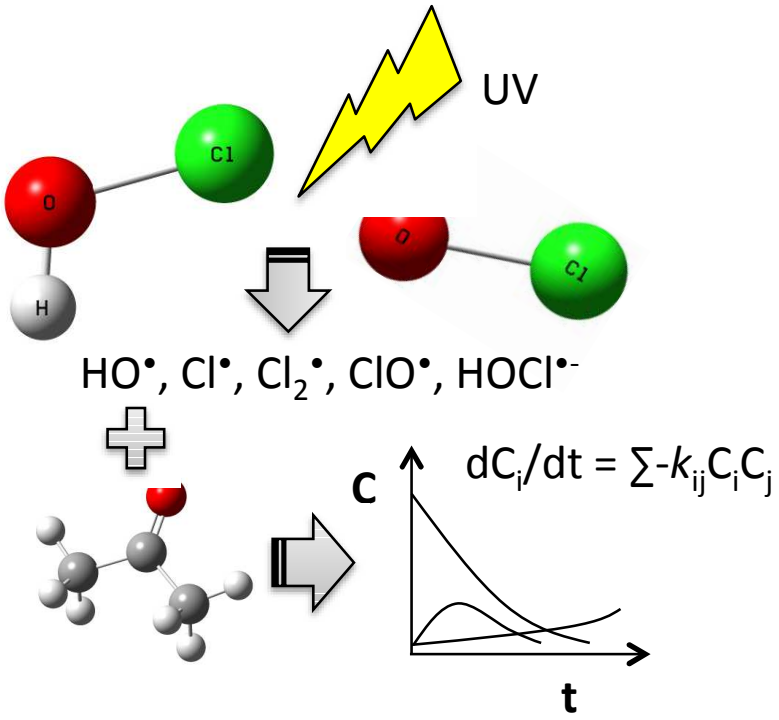

An elementary reaction based kinetic model was developed for the fate of acetone degradation in UV/free chlorine advanced oxidation process